

Article

The Influence of Different Shear Directions on the Shear Resistance Characteristics of Rock Joints

Xipeng Lai ¹, Wei Yuan ^{1,*}, Wei Wang ¹, Ruifeng Sun ², Pengzhao Du ³, Hang Lin ⁴ , Xiaodong Fu ⁵, Qinghe Niu ¹  and Chao Yin ¹

¹ School of Civil Engineering, Shijiazhuang Tiedao University, Shijiazhuang 050043, China; 1202101198@student.stdu.edu.cn (X.L.); wangweiuuu@163.com (W.W.); qinghniu@163.com (Q.N.); robinyu@bjtu.edu.cn (C.Y.)

² China Railway 17th Bureau Group Urban Construction Co., Ltd., Guiyang 550000, China; sunruifeng_zt17ju@126.com

³ Yellow River Engineering Consulting Co., Ltd., Zhengzhou 450003, China; dupz126@126.com

⁴ School of Resources and Safety Engineering, Central South University, Changsha 410083, China; hanglin@csu.edu.cn

⁵ Institute of Rock and Soil Mechanics, Chinese Academy of Sciences, Wuhan 430071, China; xdfu@whrsm.ac.cn

* Correspondence: yuanweisuper001@126.com

Abstract: The joint roughness coefficient JRC of rock joints is an important parameter for measuring the geometric morphology of rock joints. However, the parameter obtained from traditional calculation methods has certain limitations in reflecting the differences in shear strength of rock joints in different shear directions with the same orientation. Firstly, native joint surface test blocks were cast using three-dimensional reverse reconstruction technology. Subsequently, direct shear tests were conducted under different normal stress and shear direction conditions, followed by numerical simulations using the finite difference software Flac3d. The JRC coefficient calculation method proposed by Yuan was modified and extended by considering the percentage of climbing sections and the effective contact area during the ramping process. This study indicates that the numerical simulation results are in good agreement with the shear test results. The introduction of the shear climbing rate SCR and the curvature coefficient of profile CCP is used to reflect the geometric differences of the joint surfaces in different shear directions. These two parameters are nonlinearly fitted with the experimental results, leading to a calculation formula that characterizes the shear strength characteristics of the joint surfaces in different shear directions. This novel formula is an extension of the JRC–JCS model.

Keywords: JRC; shear strength; three-dimensional reverse reconstruction technology; direct shear tests; numerical simulations



Citation: Lai, X.; Yuan, W.; Wang, W.; Sun, R.; Du, P.; Lin, H.; Fu, X.; Niu, Q.; Yin, C. The Influence of Different Shear Directions on the Shear Resistance Characteristics of Rock Joints. *Buildings* **2023**, *13*, 2556. <https://doi.org/10.3390/buildings13102556>

Academic Editor: Yi Xue

Received: 21 August 2023

Revised: 24 September 2023

Accepted: 8 October 2023

Published: 10 October 2023



Copyright: © 2023 by the authors. Licensee MDPI, Basel, Switzerland. This article is an open access article distributed under the terms and conditions of the Creative Commons Attribution (CC BY) license (<https://creativecommons.org/licenses/by/4.0/>).

1. Introduction

As engineering rock masses serve as the foundation for various geotechnical structures such as roads, mines, tunnels, and dams, their mechanical characteristics significantly influence the overall stability of these constructions. The stability and overall strength of engineering rock masses are primarily governed by the shear resistance of structural surfaces at weak points within them. There are numerous factors affecting the shear resistance of these structural surfaces, with one of the most crucial being their surface topography. Natural structural surfaces exhibit varying roughness, leading to distinct mechanical properties being manifested in different shear directions during the sliding process. Therefore, researching the influence of structural surface geometry on the mechanical properties of rocks is of paramount importance.

A substantial amount of research has been carried out by scholars regarding the influence of rock joints geometry on shear strength. In 1966, F.D. Barton [1] investigated the

shear mechanical behavior of regular sawtooth-shaped structural surfaces and, based on these experiments, combined the theory of shear dilation effects with the Mohr–Coulomb criterion to propose the bilinear shear strength model. N. Barton et al. [2,3], aiming to quantify the morphological characteristics of rock joints, introduced the joint roughness coefficient (JRC) based on shear tests conducted on numerous rock joints. They also established ten standard structural profile lines for reference and developed the JRC–JCS shear strength model. The Barton formula, due to its simplicity of calculation and wide applicability, remains the most commonly used calculation formula for rock joints shear strength to this day. The traditional method of determining the magnitude of JRC values is rather subjective, and the measurement precision of the structural surface morphology data is low, with significant human error. Consequently, subsequent researchers have delved into further studies, focusing mainly on two aspects of JRC research: the acquisition of native rock joints morphology, and the correlation and quantification of morphology data with JRC. Concerning the acquisition of morphology, Develi et al. [4] developed a novel computerized mapping system for measuring the geometric morphology of rock joints, achieving a maximum accuracy of 1 mm. Jifeng et al. [5,6] devised a new type of contact perforator for the mechanized measurement of rock joints. Xia Caichu et al. [7] combined mechanized morphology measurement technology with a computer-aided testing system to create a new intelligent morphology inspection system. With the advancement of laser scanning technology, the method of obtaining rock joints morphology information transitioned from physical contact to higher-precision optical scanning. Franklin et al. [8] proposed the straightedge shading method for data acquisition by digitizing photos, while Grasselli et al. [9] collected rock joints morphology data through the ATOS structured light scanner. Since then, various types of optical scanners have become the primary tools for gathering rock joints morphology information.

Regarding how to correlate and quantify morphology data with JRC, many scholars have also conducted research in this area. Maerz et al. [10] defined the roughness profile index R_p , quantified JRC, and related it to R_p through a regression equation, ultimately establishing a new JRC calculation equation. Concerning the quantification of rock joints JRC, many researchers have also conducted relevant studies. Tse et al. [11] discretized Barton’s standard profile lines and established a functional relationship between JRC and the root mean square of the first derivative Z_2 of the joint profile slope. Zhang et al. [12] calculated JRC values by modifying Z_2 through amplitude. Yu et al. [13], based on Tse’s calculation equation, sampled JRC using different intervals to investigate the effects of spacing and derived calculation formulas for different sampling intervals. Belem et al. [14] extended the use of Z_2 into three-dimensional space and proposed quantifying rock joints morphology using the anisotropy coefficient K_a and the surface-related roughness coefficient R_s . Yuan et al. [15] defined the cumulative relative roughness amplitude (CRRA) and weighted average gradient (WAG), combining a two-dimensional profile method to develop a novel JRC calculation formula. From the aforementioned research, it can be observed that the roughness of rock joints significantly influences the peak shear strength. However, the above studies often apply to rough calculations of JRC in a single shear direction, and do not consider the effective contact during the shear process.

For this reason, this paper selects the native rock joints and prints six rock joints counterclockwise at 30° intervals in the direction of $0\text{--}150^\circ$ using 3D inverse reconstruction technology. It carries out the direct shear test in the same orientation with different shear directions and different normal stresses to simulate the shear damage of the rock joints of the fracture-bearing engineered rock. Numerical simulations were performed using the finite difference software Flac3d, and the test and simulation result data were compared to verify the reliability of the test. The shear climbing rate (SCR) and curvature coefficient of profile (CCP) are proposed to supplement and modify the JRC calculation method proposed by Yuan through nonlinear surface fitting. Finally, a model is constructed to calculate the shear strength of rock joints under different shear directions with different surface roughness and different normal stresses.

2. Construction of the Shear Model

To investigate the shear strength characteristics of rock joints within the test specimens, this experiment employs the constant normal load (CNL) shear test to assess the shear resistance of different surface morphology rock joints under varying levels of normal stress. However, due to the limited availability of natural rock formations for experimentation, coupled with their diverse surface irregularities and types, the approach involves selecting native engineering rock masses containing rock joints as the subjects of study. Brittle cement mortar specimens are cast on-site to possess similar surface morphology and mechanical properties to the identified rock joints.

The pouring process is illustrated in Figure 1. Utilizing the EinScan-Pro handheld high-precision scanner (Manufactured by Shining 3D, Hangzhou, China), the surface morphology of the rock joints is scanned and recorded, transforming the scan data into high-precision point cloud data. Through reverse engineering software such as Rhino and Wrap, a mesh model is constructed that closely resembles the native surface morphology of the structure. In this study, six orientations and twelve shear directions ($0^\circ, 30^\circ, 60^\circ, 90^\circ, 120^\circ, 150^\circ, 180^\circ, 210^\circ, 240^\circ, 270^\circ, 300^\circ, 330^\circ$) were selected for sampling (directions and cutting dimensions depicted in Figure 1c). Furthermore, utilizing the HORI dual-nozzle large-scale resin 3D printer, a total of six rock joints molds were fabricated.

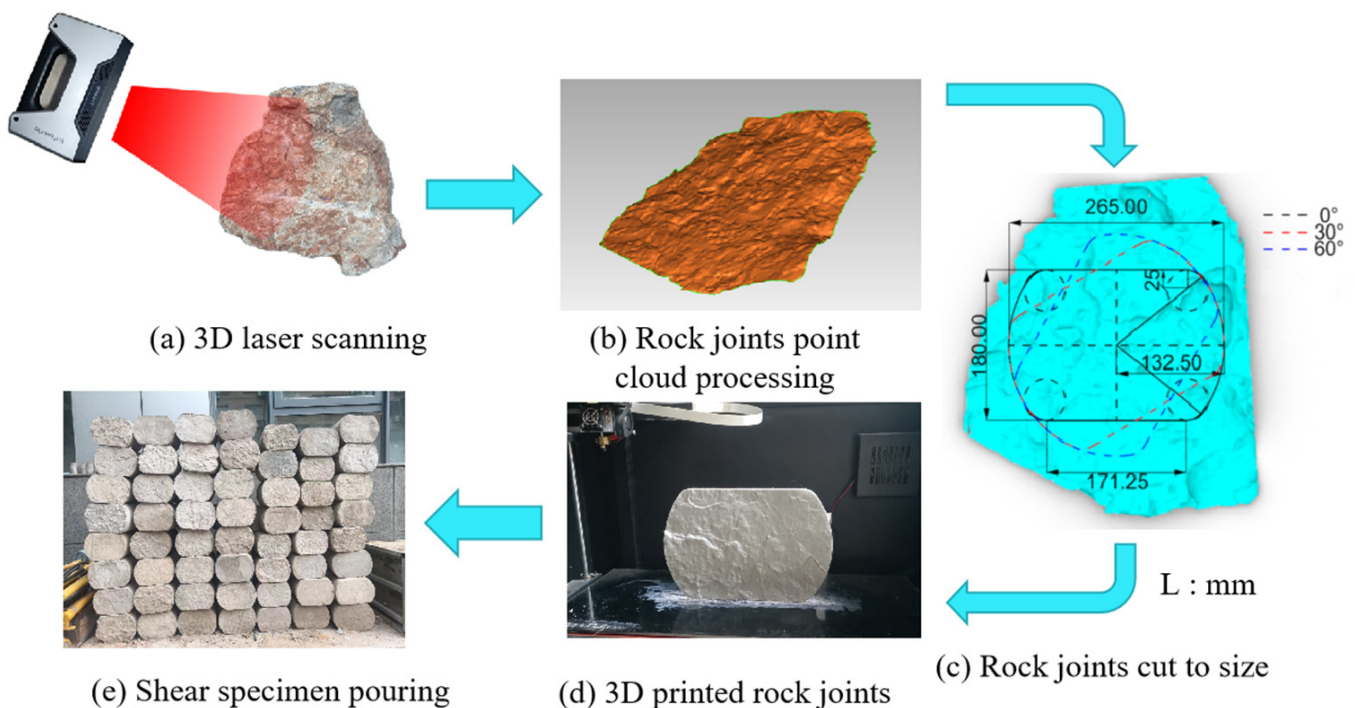


Figure 1. The manual specimen casting process.

Due to the intricate and non-repetitive nature of natural joint surface morphology, this study employs replicas made of cementitious mortar as substitutes for experimental purposes, water, Portland cement, fine sand, and other materials that are used for proper design matching. According to the proposed strength classification for rocks, cement mortar with three strengths (soft: 5~15 MPa, medium-hard: 15~30 MPa, and hard: 30~60 MPa) is planned to be poured as test specimens. These test groups are represented by code combinations S-S, M-M, and H-H, where S represents soft rock, M represents medium-hard rock, and H represents hard rock. After curing for 28 days, conventional triaxial tests, Brazilian splitting tests, and uniaxial compression tests are conducted to obtain the corresponding basic mechanical parameters of the artificial rock mass. The basic mechanical parameters of the three strength test specimens are shown in Table 1 after testing.

Table 1. Basic mechanical parameters of artificial rock mass.

Rock Type	Contents (%)			σ_c (MPa)	φ (°)	c (MPa)	E (GPa)
	Water	Cement	Sand				
Soft (S)	20	40	40	14.82	36.3	4.12	3.12
Medium-hard (M)	18.8	47.2	34	25.70	37.2	6.26	4.53
Hard (H)	16.7	50	33.3	35.21	38.5	9.3	5.56

σ_c —Compressive strength of the material. φ —Internal friction angle of the rock mass. c—Cohesion. E—Elastic modulus of the material.

3. Indoor Test and Numerical Simulation

3.1. Direct Shear Test

This experiment entails casting three different strength combinations of test specimens in each direction, with three repetitions for each combination to carry out tests under three levels of normal stress. Ultimately, a total of 108 samples are cast across twelve shear directions to facilitate the testing process. The shear test was carried out on the poured samples using the anchorage performance tester for anchored structural surfaces (Figure 2). Normal stresses of 1.0 MPa, 2.0 MPa, and 3.0 MPa were respectively applied to each identical rock joint before performing the shear test. An electronic dial indicator was used to measure the shear and normal displacements of the sample. The shear force loading was carried out stepwise at a displacement rate of 0.02 mm/step and stopped when the shear displacement reached 6 mm. The horizontal shear stress corresponding to each displacement was recorded throughout the test, and the shear stress versus shear displacement curve was plotted to analyze the characteristics of each stage. The basic friction angle φ_b of the rock joints under different combinations was determined through direct shear tests on flat rock joints. It should be noted that this friction angle differs from the internal friction angle of the rock mass, as it specifically refers to the friction angle of the rock joints within the rock mass. Analysis of the data presented in Table 2 reveals a positive correlation between the friction angle of the rock joints and the uniaxial compressive strength of the rock. This finding serves as evidence for the necessity of considering uniaxial compressive strength as a variable in studying shear strength.

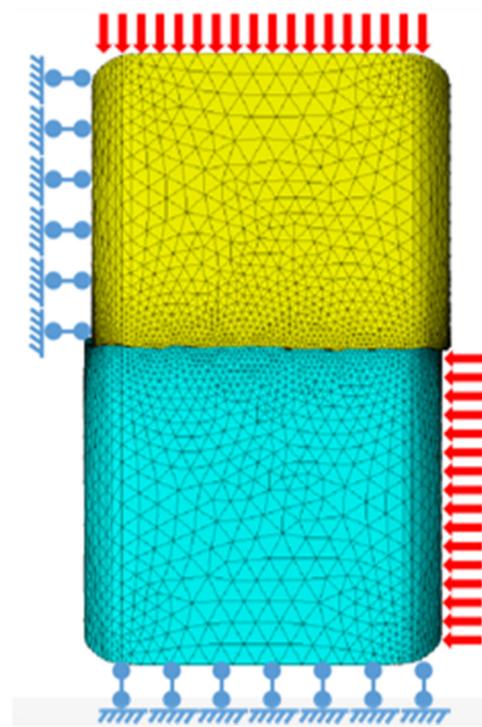
**Figure 2.** Installation of anchorage performance tester and accessories for anchored structural plane.

3.2. Numerical Simulation

The scanned point cloud files were post-processed using Rhino modeling software to establish a sheared rock block grid model. The finite difference software (Flac3d) was used to perform numerical simulations of engineering rock mass shearing. The shearing simulation constraints are shown in Figure 3. The blue part represents the constraint end, and the red arrows represent the location where normal stress and shear rate are applied.

Table 2. Selection of simulation parameters of the rock joints in 0° direction.

Specimen	S-S			M-M			H-H		
Normal stress (MPa)	1	2	3	1	2	3	1	2	3
Normal stiffness (GPa·m ⁻¹)	29.41	61.17	100.62	42.41	83.05	123.03	53.79	105.26	141.40
Shear stiffness (GPa·m ⁻¹)	3.20	6.12	8.42	4.20	8.61	11.66	4.82	10.33	16.02
φ_b (°)		30.4			32.48			34.35	

**Figure 3.** Boundary conditions for joint shear simulation.

In the natural state, in order to more realistically simulate the shearing of the rock blocks, and considering the integrity and weathering degree of the rock blocks, the numerical model of the rock blocks adopts the Hoek–Brown model, and the relevant parameters of the rock mass are selected by Table 1. A simulated interface is established between the upper and lower rock blocks, the relevant parameters of the simulated interface are selected by Table 2, wherein the normal stiffness and shear stiffness of the interface are obtained through rock mechanics experiments.

This paper uses the method proposed by Bandis et al. [16] to calculate the normal stiffness k_n , and conducts compression tests on specimens with and without rock joints to plot the compression curves. The displacement difference of the compression curves and the corresponding normal stress under the two conditions are used to obtain the closed deformation diagram. The variables include the compression displacement of specimens without structural planes (V_s), the compression displacement of specimens with structural planes (V_j), maximum closure (V_m), and the normal stiffness of the structural planes (k_{ni}) under a certain normal stress σ_i . The calculation schematic is shown in Figure 4.

For the value of the shear stiffness k_s , the method proposed by Vallier et al. [17] was used to calibrate the tangential stiffness by taking the slope of a point on the elastic section of the shear stress versus the shear displacement curve, before reaching the peak shear strength τ_p . The calculation is schematically shown in Figure 5.

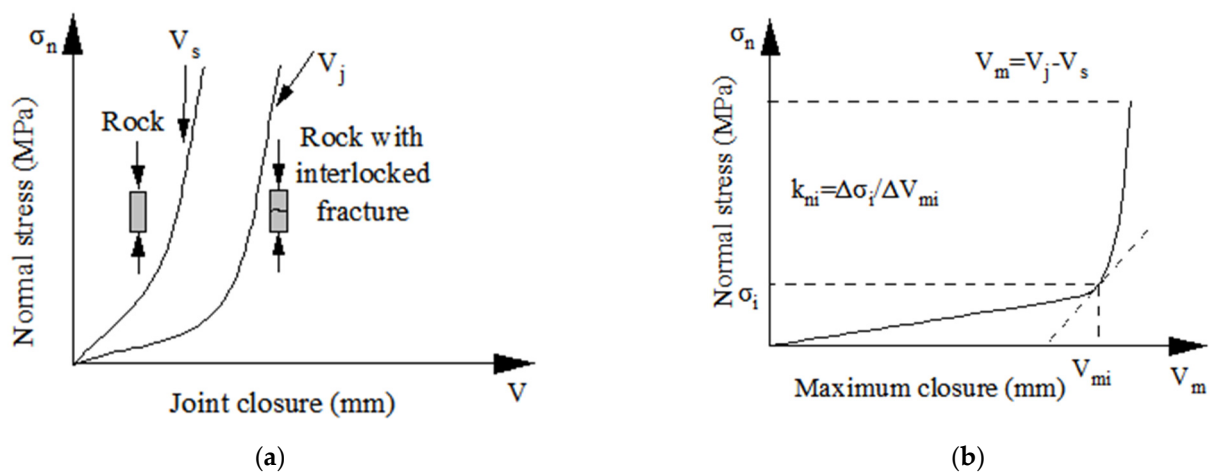


Figure 4. Schematic diagram of normal stiffness calculation: (a) normal stress vs deformation relations of intact and fractured specimens; (b) maximum closure V_m calculation chart.

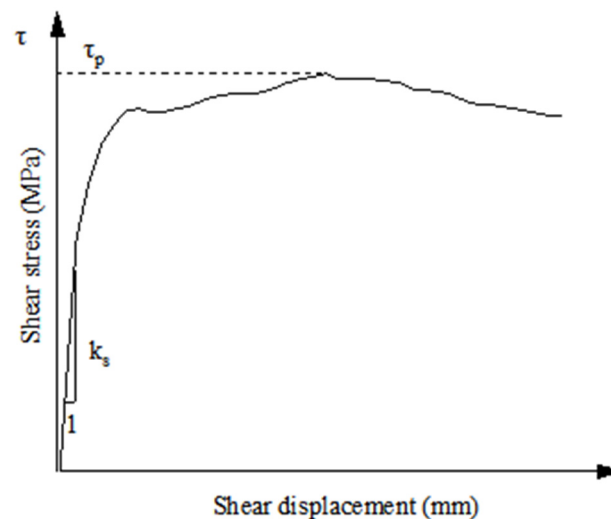


Figure 5. Schematic diagram of shear stiffness calculation.

Since the rock joints go through the rock blocks without any filling, the cohesive force, overall tensile strength, and shear expansion angle of the rock joints are set to 0. The final simulated shear rate is adjusted to 1×10^{-6} m/step, and the relevant parameters of the rock joints are listed in Table 2.

3.3. Analysis of Test and Simulation Results

Figure 6 shows the stress cloud map during the shearing process of the specimen, where positive values represent tensile stress and negative values represent compressive stress. Specifically, the shearing process can be divided into four stages. Stage 1 is the gap bonding stage, during which local areas between the rock joints start to generate compressive stress and gradually spread. Stage 2 is the linear elastic stage of shearing, as can be observed from the figure, where the rock joints undergo elastic deformation and there are a few cracks uniformly present. Stage 3 is the stage of non-uniform crack development, where the contact between some rock joints is no longer complete, resulting in stress concentration at some contact points, and the accelerated expansion of cracks until the mutual penetration and failure of the rock mass. Stage 4 is the residual shearing stage, where new fracture surfaces generate sliding friction due to the relative movement of rock blocks and normal stresses from above. At the same time, slight interlocking occurs

between residual edges of different fracture surfaces, leading to stress concentration (see the magnified image in the bottom right corner of Figure 6).

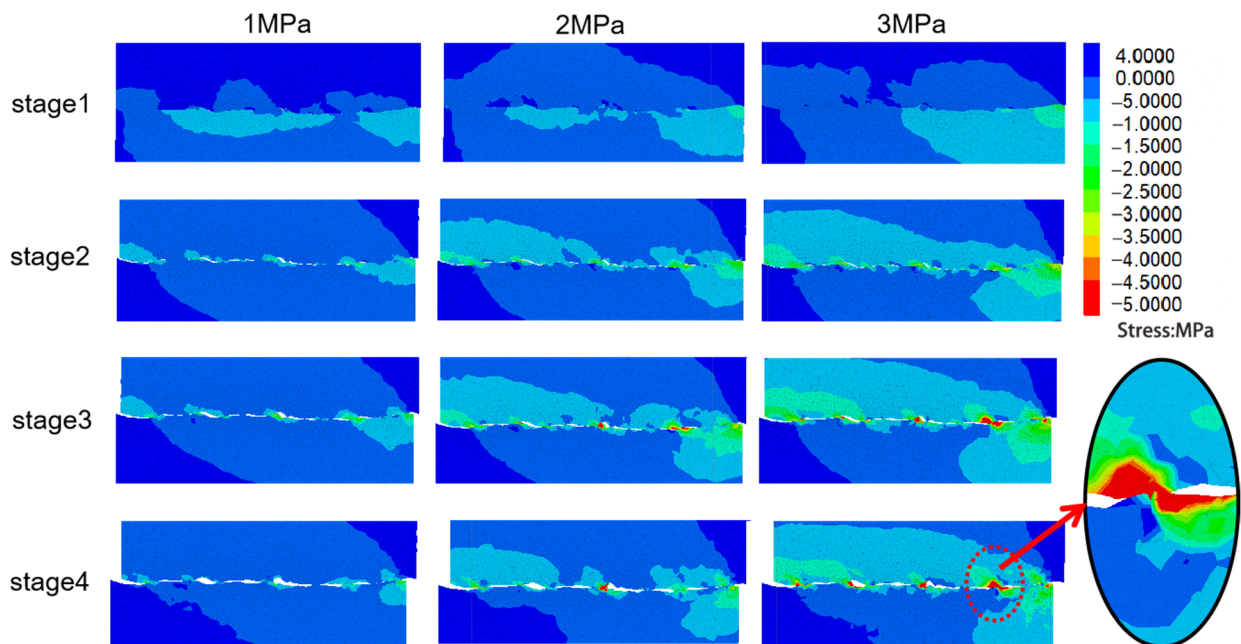


Figure 6. Shear stress variation diagram under different conditions.

The rock joints exhibited the ultimate failure condition after undergoing four stages, as shown in Figure 7. The red region in Figure 7a represents the plastic shear zone, where severe shear deformation occurred in the raised area of the rock joints. This confirms that it is a localized region of shear stress concentration, which primarily bears the shear resistance of the rock joints. Furthermore, Figure 7b also reveals the wear and failure condition of the raised area during indoor testing, with the upper region exhibiting more prominent damage. This is attributed to it being the shear end region, where a lack of constraint results in weaker shear resistance. Consequently, it is the first to fail and experiences the most severe damage during the shearing process. This phenomenon aligns with the characteristic shear failure of interconnected rock joints.

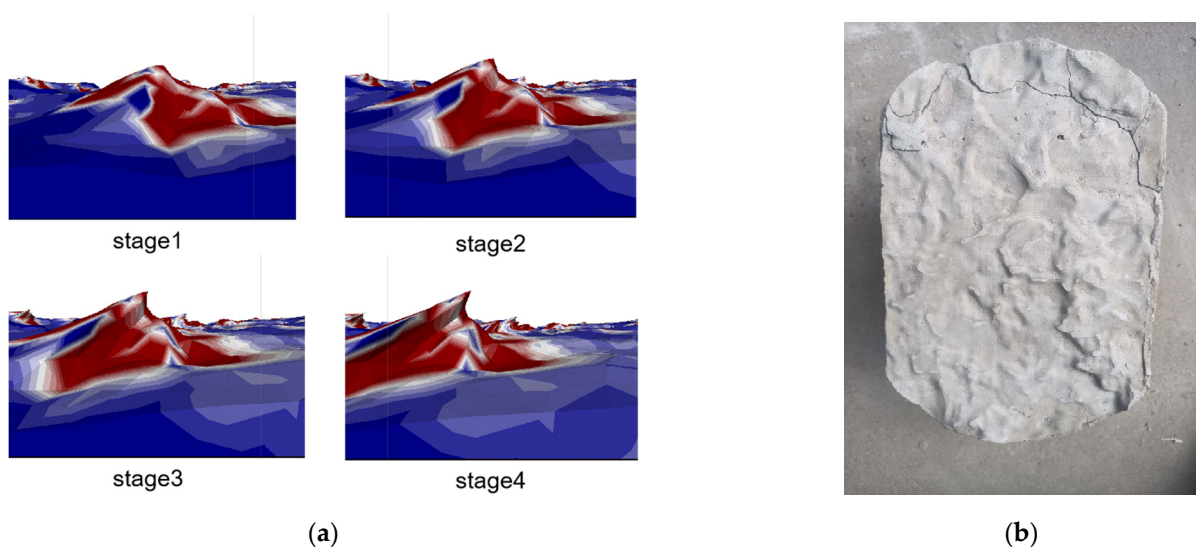


Figure 7. Shear failure condition: (a) shearing damage process, (b) shear-damaged surface.

The stress–displacement comparison curve for the 0° direction S–S combination in Figure 8a demonstrates that the direct shear test and simulation results follow the same pattern. As the normal stress applied to the rock joints increases, the peak shear strength also increases, along with the residual shear strength and tangential stiffness of the rock joints, which are positively correlated with the normal stress. Figure 8b–d presents the peak shear strength comparison graphs for S–S, M–M, and H–H combinations. From these graphs, it is evident that the peak shear strength varies significantly for different shear directions of the rock joints. However, in the traditional JRC determination method, the standard profile line used for different shear directions with the same orientation is identical, leading to identical JRC values. Nevertheless, based on the experimental results shown in Figure 8b–d, it can be observed that under unchanged conditions, although the same JRC value is selected for rock joints with the same orientation during calculations, there are visible differences in the peak shear strength. Therefore, further research and exploration are needed to quantitatively determine JRC.

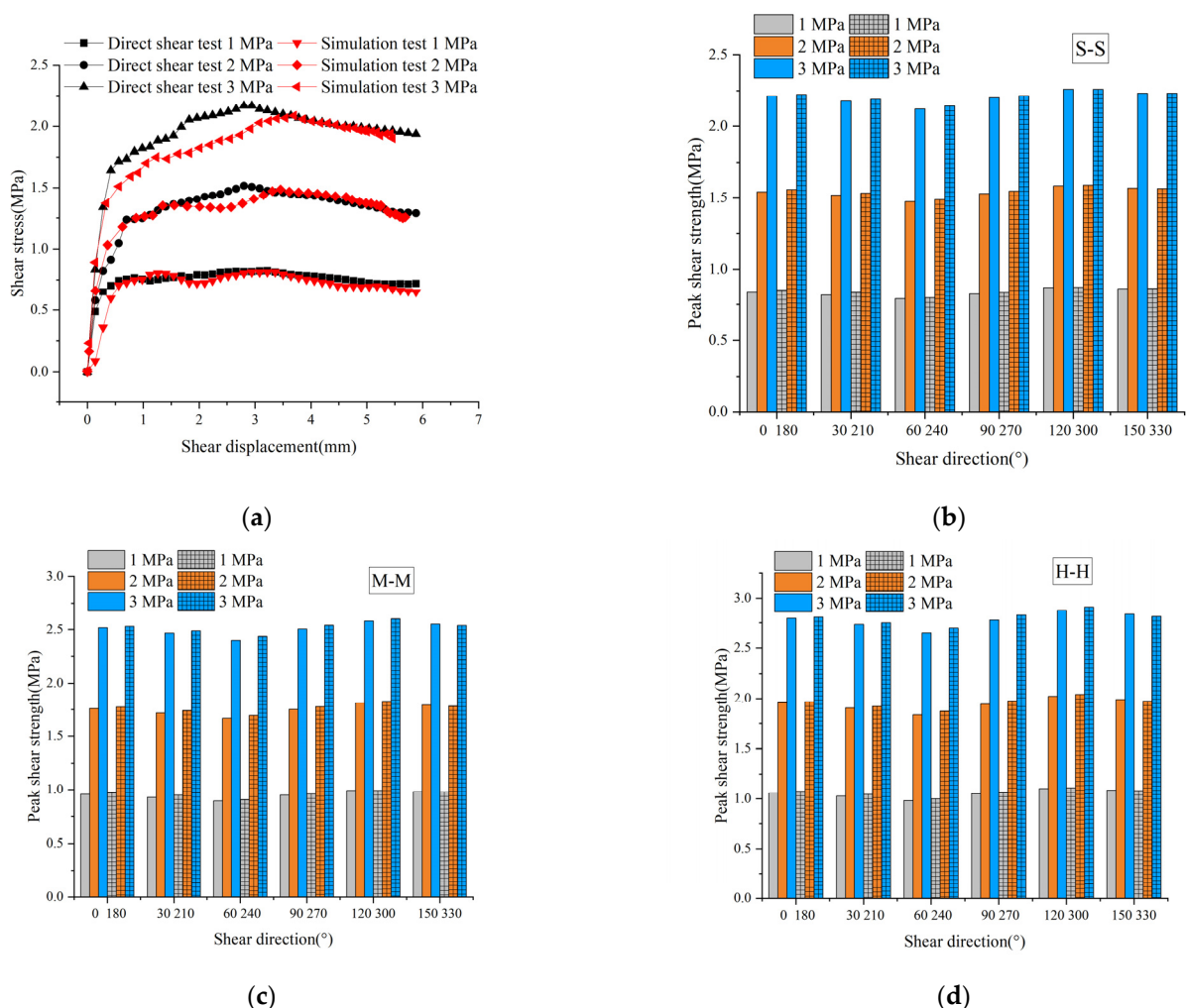


Figure 8. Peak shear strength comparison chart: (a) The stress–displacement comparison curve, (b–d) comparison of peak shear strength for different shear directions in S-S, M-M, and H-H combination.

4. Establishment of Shear Mechanics Model

In early studies on the shear strength of rock joints, many scholars quantified the basic mechanical parameters of rock joints and established a mathematical relationship between them and the peak shear strength to explore the rock shear mechanism. N. Barton established the JRC–JCS shear model by analyzing a large number of rock joints shear test

results. This model can represent rock joints shear performance with low normal stress and minor undulations properties. Its expression is:

$$\tau_p = \sigma_n \tan \left[\varphi_b + \text{JRC} \lg \left(\frac{\text{JCS}}{\sigma_n} \right) \right] \quad (1)$$

where τ_p is the peak shear strength of rock joints, σ_n is the normal stress; φ_b is the basic friction angle, JRC is the joint roughness coefficient, and JCS is the joint wall compressive strength.

It can be seen from Equation (1) that the peak shear strength is related to many factors. The normal stress σ_n can be derived from the total stress of the upper layer on the rock joints. The basic friction angle φ_b can be obtained from direct shear experiments. Regarding the JCS, it can be equivalent to the uniaxial compressive strength of the rock when the degree of rock weathering is low. As for the JRC, in actual engineering, the known profile is often decomposed into lines. Compared with the 10 standard profile lines drawn by Barton, this method is highly subjective and may lead to significant errors in the results. Therefore, it is necessary to establish a correct method of quantitative analysis.

Quantification of Structural Surface Geometry

Reference Yuan et al. [15] proposed a method to dissect the rock joints through a two-dimensional profile line (Figure 9). The cumulative relative undulation amplitude CRRA is defined to characterize the climbing effect of shear strength considering the scale effect, while using the weighted average gradient WAG to characterize the rock joints friction effect, and finally, nonlinearly fitting the two metrics to derive the quantification method of JRC.

$$\text{WAG} = \frac{\sum_{i=1}^n |z_{i+1} - z_i| \sqrt{1 + \left| \frac{z_{i+1} - z_i}{x_{i+1} - x_i} \right|^2}}{\sum_{i=1}^n |x_{i+1} - x_i| \sqrt{1 + \left| \frac{z_{i+1} - z_i}{x_{i+1} - x_i} \right|^2}} \quad (2)$$

$$\text{CRRA} = \frac{1}{L} \sum_{i=1}^n |z_{i+1} - z_i| \quad (3)$$

$$\text{JRC}_{\text{Yuan}} = p_1 e^{\text{CRRA} \times \text{WAG}} + p_2 \times \text{CRRA} + p_3 \times \text{WAG} \quad (4)$$

where $z_{i+1} - z_i$ is the height difference between two adjacent sampling points, $x_{i+1} - x_i$ is the sampling interval, n is the number of intervals, L is the length of the shear profile line, and p_1, p_2, p_3 are the corresponding empirical coefficients under different sampling intervals.

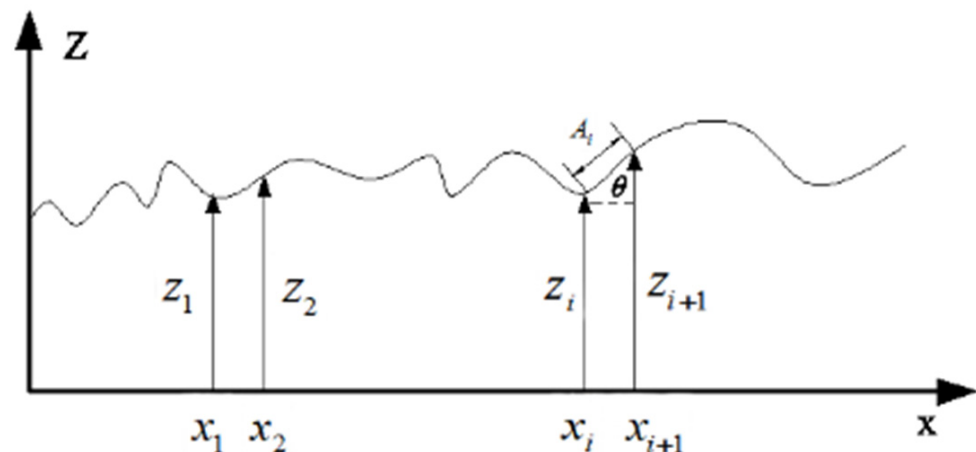


Figure 9. Schematic diagram of 2D section line index calculation.

According to the recommendation (the sampling interval should be shorter than $L/120$), this paper uses $L/140$ as the sampling interval and extracts 11 section lines at equal intervals on the shear section in the Y-axis direction to divide the rock joints into 10 equal-width regions, as shown in Figure 10a,b. The average CRRA and WAG values are obtained using the above Equations (2) and (3) and the following Equations (5) and (6):

$$WAG_{ave} = \frac{1}{n} \sum_{t=1}^n WAG_t \quad (5)$$

$$CRR_{ave} = \frac{1}{n} \sum_{t=1}^n CRR_t \quad (6)$$

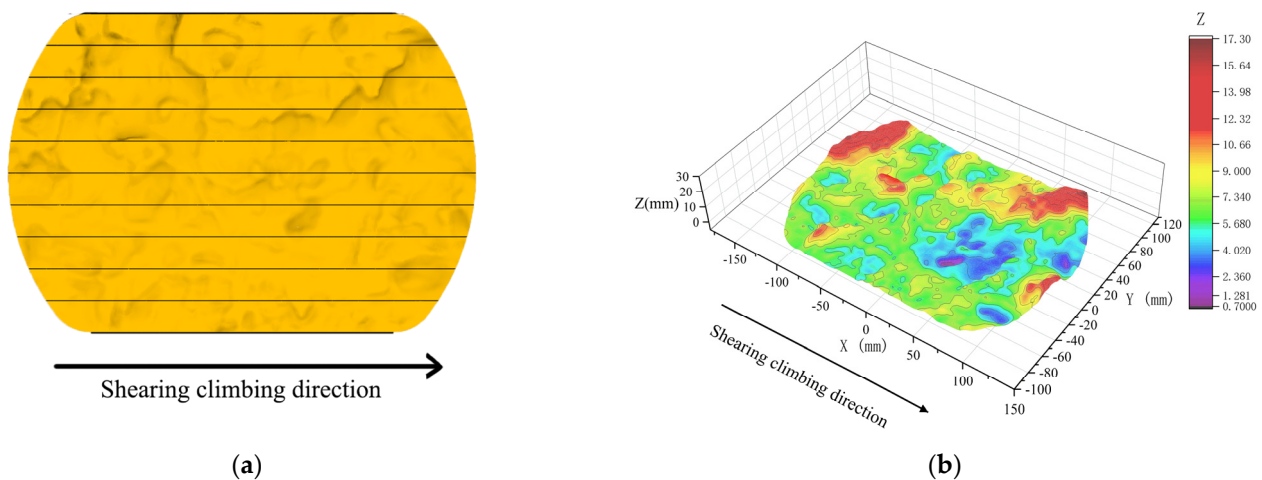


Figure 10. Schematic diagram of the rock joint 3D printing area: (a) profile line selection; (b) rock joint morphology information.

Bring the required dimensionless index into Equation (4), and refer to the empirical coefficient table under the corresponding sampling interval in Yuan et al. [15] to obtain the values of p_1 , p_2 , and p_3 (shown in Table 3). Finally, the calculated values of JRC in the directions of $0^\circ/180^\circ$, $30^\circ/210^\circ$, $60^\circ/240^\circ$, $90^\circ/270^\circ$, $120^\circ/300^\circ$, and $150^\circ/330^\circ$ are 7.820, 7.230, 6.420, 7.668, 8.552, and 8.145, respectively.

Table 3. Experience coefficient corresponding to interval $L/140$.

Sampling Numbers	p_1	p_2	p_3
140	-1.2668	106.0937	-41.6964

Data source: Yuan et al. [15].

Based on the aforementioned Barton formula, the values of σ_n , JCS, and φ_b are substituted into the equation to obtain the inverse calculation of JRC. The outliers in the corresponding shear direction are eliminated, and the remaining values are summed and averaged to obtain the final calculation result. Table 4 presents the JRC values calculated using these two methods. Additionally, the ratio α between the inverse calculation value and Yuan's calculation formula is included in the third row. From the table, it can be observed that there are certain differences in the JRC values of the rock joints under different shear directions.

Table 4. Comparison chart of JRC values for different shear directions.

	Shear Direction/°											
	0°	30°	60°	90°	120°	150°	180°	210°	240°	270°	300°	330°
Inverse calculation	8.168	7.576	6.703	7.974	8.953	8.626	8.392	7.883	7.079	8.312	9.088	8.526
Yuan	7.820	7.230	6.420	7.668	8.552	8.145	7.820	7.230	6.420	7.668	8.552	8.145
α	1.0445	1.0479	1.0441	1.0399	1.0469	1.0591	1.0731	1.0903	1.1026	1.0840	1.0626	1.0468

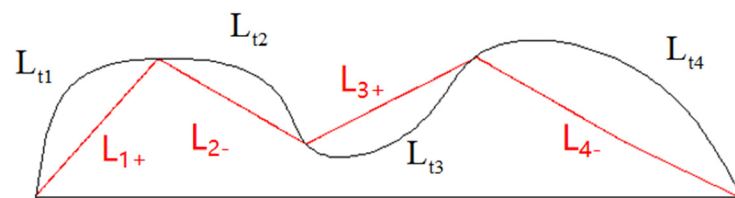
Based on the analysis in Section 3.3, the morphology features and contact conditions of rock joints are analyzed from both macroscopic and microscopic perspectives. From a macroscopic viewpoint, the profile lines exhibit both climbing and non-climbing sections. In the discretization process, a climbing section is defined as when $z_{i+1} \geq z_i$, while a non-climbing section is defined as when $z_{i+1} < z_i$; non-climbing sections of through-type rock joints do not contribute significantly to shear strength. This paper proposes using the ratio between the length of the discretized climbing sections and the total length of the profile lines (L_p) as the shear climbing rate (SCR) to reflect their contribution. From a microscopic perspective, there are certain morphological differences between straight and smooth sampled sections and real rock joints profiles. Pikens and Gurland [18] defined the curvature index P_s to quantitatively characterize the bending of rock joints. This paper converts its surface equivalent value into two-dimensional space and defines it as the curvature coefficient of profile (CCP), which represents the ratio between the actual length of a profile line segment and its corresponding sampled section length. The specific calculation steps can be seen in Figure 11 and Equations (7)–(9).

$$L_p = \sum_{i=1}^n L_{i+} + \sum_{i=1}^n L_{i-} \quad (7)$$

$$\text{SCR} = \frac{1}{L_p} \sum_{i=1}^n L_{i+} \quad (8)$$

$$\text{CCP} = \frac{1}{n} \left(\sum_{i=1}^n \frac{L_{ti}}{L_{i+}} + \sum_{i=1}^n \frac{L_{ti}}{L_{i-}} \right) \quad (9)$$

where L_p is the total length of the profile lines, L_{ti} is the microsegment length of the i -th profile line after discretization, L_{i+} is the length of the i -th discretized climbing section, and L_{i-} is the length of the i -th discretized non-climbing section.

**Figure 11.** Schematic diagram of profile line discretization.

The relationship among α , SCR, and CCP, as indicated by Equation (10), was discovered through computational analysis. A nonlinear surface fitting was then performed to explore the interconnection between these three variables. The resultant fit is depicted in Figure 12, showcasing a favorable fitting outcome. The coefficient of determination R^2 equals 0.9773, while the correlation coefficients b , c , and d are found to be 0.67, -1.53 , and 3.07, the relationship between the newly proposed JRC calculation formula and the Yuan formula can be seen in Equation (11), respectively:

$$\alpha = b \times \ln(\text{SCR}) + c \times \text{CCP} + d \quad (10)$$

$$JRC_{New} = \alpha \times JRC_{Yuan} \quad (11)$$

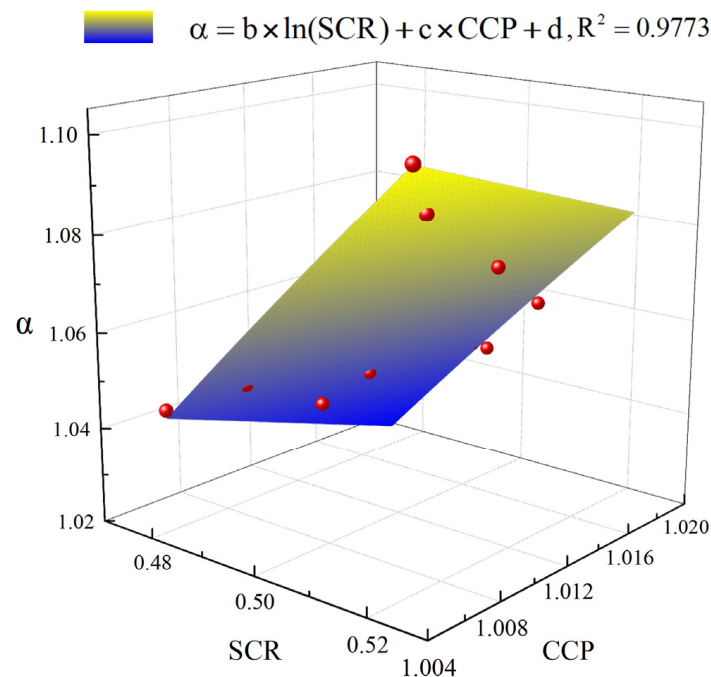


Figure 12. Multivariate nonlinear fitting.

5. Comparison and Validation of Formulas

Zhao et al. [19] incorporated Barton's proposed ten criteria for profile line morphology into Matlab, enabling the computation of the root mean square of the first derivative of the contour lines, denoted as Z_2 . By applying a fitting procedure, an empirical calculation formula for JRC was obtained. The computation method is presented in Equations (12) and (13):

$$Z_2 = \left[\frac{1}{L} \sum_{i=1}^L \frac{(y_{i+1} - y_i)^2}{Vx} \right]^{\frac{1}{2}} \quad (12)$$

$$JRC_{Zhao} = 32 + 33.63 \lg(Z_2) \quad (13)$$

where y is the height of the shear profile line, Δx is the sampling interval, and L is the projected length of the contour lines along the X-axis.

To validate the reliability of the formulas presented in this article, the calculated JRC values obtained from the Yuan formula, Zhao formula, and the newly proposed formula are substituted into the Barton formula. The final computed results are then compared with the direct shear test (shown in Figure 13). By analyzing the distribution of the increasing and decreasing intervals of the curve in the figure, it can be observed that all three calculation methods yield consistent results regarding the shear characteristics of the rock joints in different directions. Specifically, the intervals from 60° to 120° and 240° to 300° demonstrate an increase, while the remaining intervals show a decrease. Compared to the conventional method of calculating JRC using Z_2 values, the Yuan formula introduces two parameters, CRRA and WAG, which better reflect the climbing and friction effects during the shear process and align more closely with reality. However, it still underestimates the experimental values and exhibits certain discrepancies. Furthermore, it fails to capture the differences in shear directions for the same orientation. In this study, by introducing two coefficients, SCR and CCP, to modify the Yuan formula, both of these issues have been addressed.

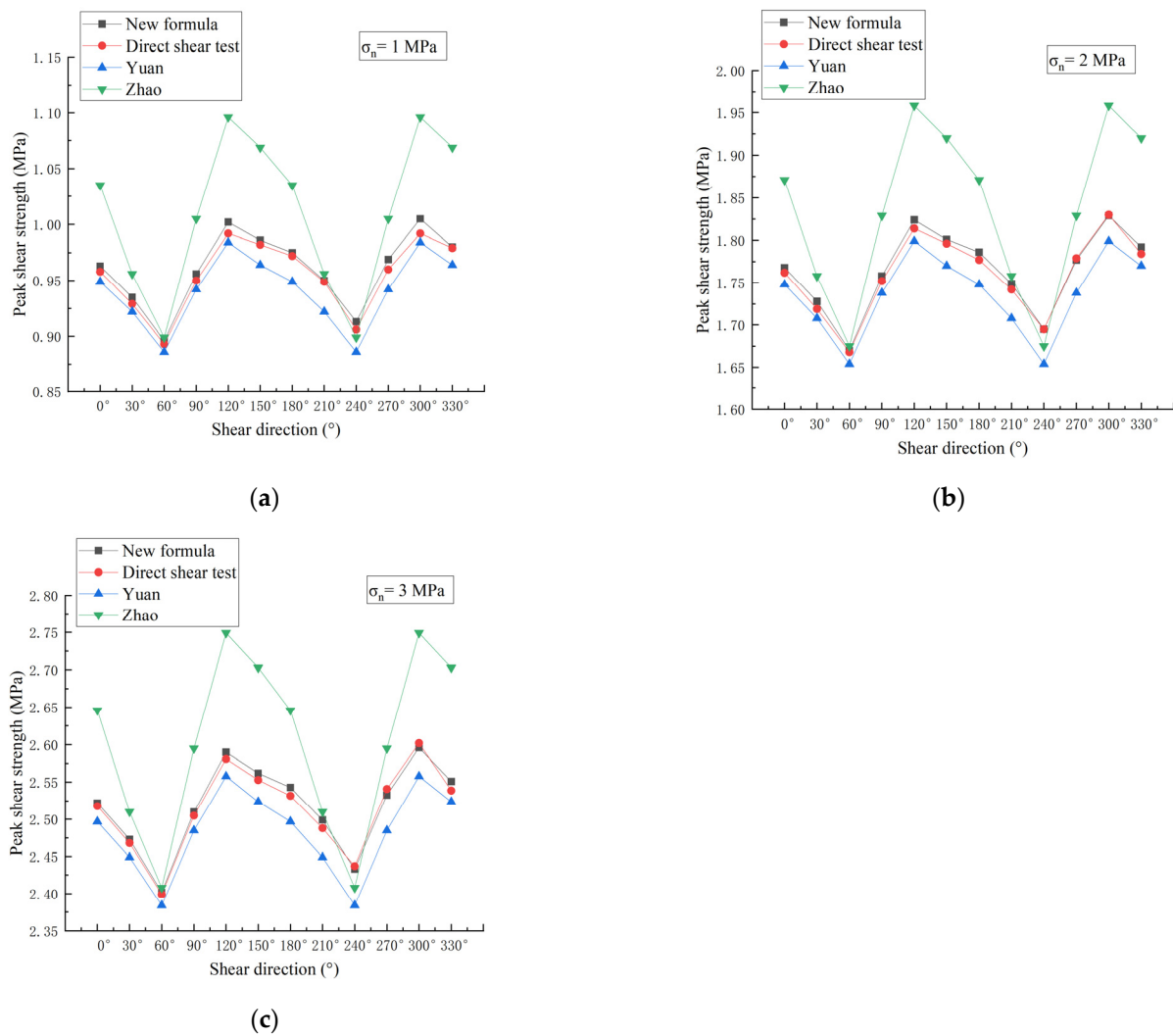


Figure 13. Comparison chart of calculation results: (a–c) Values of peak shear strength in different shear directions under normal stress conditions of 1 MPa, 2 MPa, and 3 MPa.

To depict the disparities between the calculated values and direct shear test values more accurately, this paper employs the formula of mean deviation (shown in Equation (13)) to describe the deviations between these three calculated values and the direct shear test values. The Yuan formula yields a deviation of 1.7%, the Zhao formula yields 4.9%, and the newly proposed formula in this study yields a deviation of 0.61%. Based on the aforementioned analysis and data, it is evident that the modification of the Yuan formula presented in this paper significantly enhances the accuracy of the peak shear strength calculation.

Where σ_{ave} is the average deviation, n is the number of samples, and τ_{pt} is the peak shear strength test value, τ_{pc} is the theoretically calculated value of the peak shear strength.

6. Conclusions

Using three-dimensional reverse reconstruction technology, the surface morphology point cloud data of the rock joints are scanned and obtained. The 3D-printed molds are then used to cast cement mortar specimens. Direct shear tests under different normal stresses and finite difference numerical simulations are conducted to obtain the shear strength curves of the rock joints. Finally, based on the Barton model for rock joints shear strength and the JRC calculation formula proposed by Yuan, an analysis of the shear characteristics of the rock joints in different shear directions is conducted, leading to the following conclusions:

- (a) The shear process of the rock joints is simulated proportionally using the finite difference software Flac3d. The simulation results are in good agreement with the indoor direct shear test results. It can be concluded that the shear process can be roughly divided into stages of gap bonding, linear elastic, non-uniform crack development, and residual shearing. The stress distribution and failure behavior of the rock joints vary in different stages. The protrusions on the rock joints are the main areas responsible for shear resistance, and the contact conditions at these protrusions have a certain influence on the shear strength of the rock joints. At the shear end, due to lack of restraint, it is the first to fail and exhibits the most severe damage.
- (b) The geometric morphology of the rock joints is quantified using a two-dimensional profiling method, and an inverse calculation of JRC values is performed based on experimental results. A comparison is made with Yuan's calculation method, and modifications and extensions are made to Yuan's formula by introducing the shear climbing rate (SCR) and curvature coefficient of profile (CCP). Finally, a new calculation formula for the shear strength of rock joints is established based on Barton's formula.
- (c) A method for calculating JRC values using Z_2 is introduced, and it is compared with Yuan's formula and the modified formula proposed in this study. The applicability of these three methods for calculating the shear strength of rock joints is demonstrated, and the average deviation between the three formulas and experimental values is calculated. The analysis results show that the three formulas can, to some extent, reflect the variation of the shear strength of rock joints with shear direction. However, the modified formula proposed in this study can better reflect the differences in shear strength of the same orientation in different shear directions, and it has the smallest average deviation from the experimental values.

Author Contributions: Conceptualization, X.L. and W.Y.; Methodology, X.L., W.Y. and R.S.; Software, X.L. and W.Y.; Investigation, X.L., W.Y., W.W., R.S. and P.D.; Data curation, X.L., W.Y., H.L., X.F., Q.N. and C.Y.; Writing—original draft, X.F.; Writing—review & editing, W.Y. and X.L.; Visualization, X.L. and W.Y.; Project administration, W.Y.; Funding acquisition, W.Y. All authors have read and agreed to the published version of the manuscript.

Funding: The authors gratefully acknowledge the support by the Key Research and Development Program of Hebei Province (Grant NO. 22375402D,22375420D), The Natural Science Foundation of Hebei Province, China (Grant NO. E2021210041), The Natural Science Foundation of Hunan Province, China (Grant NO. 2022JJ30641), Hebei Natural Science Foundation (Grant NO. E2021210128).

Institutional Review Board Statement: Not applicable.

Informed Consent Statement: Informed consent was obtained from all subjects involved in the study.

Data Availability Statement: Some or all data, models, or code generated or used during the study are available from the corresponding author by request.

Acknowledgments: We appreciate the editors and reviewers for providing constructive and careful comments that significantly improved the manuscript.

Conflicts of Interest: The authors declare that the research was conducted in the absence of any commercial or financial relationships that could be construed as a potential conflict of interest.

References

1. Patton, F.D. Multiple modes of shear failure in rock. In Proceedings of the 1st Congress of International Society of Rock Mechanics, Lisbon, Portugal, 25 September–1 October 1966.
2. Barton, N. Review of a new shear-strength criterion for rock joints. *Eng. Geol.* **1973**, *7*, 287–332. [[CrossRef](#)]
3. Barton, N.; Choubey, V. The shear strength of rock joints in theory and practice. *Rock Mech.* **1977**, *10*, 1–54. [[CrossRef](#)]
4. Develi, K.; Babadagli, T.; Comlekci, C. A new computer-controlled surface-scanning device for measurement of fracture surface roughness. *Comput. Geosci.* **2001**, *27*, 265–277. [[CrossRef](#)]
5. Ji, F.; Shi, Y.C.; Feng, K.W. A new measurement of rock joints surface—Contact punching device. In Proceedings of the 3rd Conference of Geo-Engineering, Chengdu, China, 11 June 2009.

6. Ji, F.; Shi, Y.C. A study of the measuring and strength size effect of the surface shape of structure plane. *Hydrogeol. Eng. Geol.* **2011**, *38*, 63–67. [[CrossRef](#)]
7. Xia, C.C.; Sun, Z.Q. RSP-1 type intelligent profilometer of rock surface. *J. Hydraul. Eng.* **1995**, *5*, 62–66.
8. Franklin, A.J.; Maerz, H.N.; Bennett, P.C. Rock mass characterization using photoanalysis. *Int. J. Min. Geol. Eng.* **1988**, *6*, 97–112.
9. Grasselli, G. Shear Strength of Rock Joints Based on Quantified Surface Description. *Rock Mech. Rock Eng.* **2006**, *39*, 295–314. [[CrossRef](#)]
10. Maerz, N.H.; Franklin, J.A.; Bennett, P.C. Joint roughness measurement using shadow profilometry. *Int. J. Rock Mech. Min. Sci. Geomech. Abstr.* **1990**, *27*, 329–343.
11. Tse, R.; Cruden, D.M. Estimating joint roughness coefficients. *Int. J. Rock Mech. Min. Sci. Geomech. Abstr.* **1979**, *16*, 303–307. [[CrossRef](#)]
12. Zhang, G.; Karakus, M.; Tang, H.; Ge, Y.; Zhang, L. A new method estimating the 2D Joint Roughness Coefficient for discontinuity surfaces in rock masses. *Int. J. Rock Mech. Min. Sci.* **2014**, *72*, 191–198. [[CrossRef](#)]
13. Yu, X.; Vayssade, B. Joint profiles and their roughness parameters. *Int. J. Rock Mech. Min. Sci. Geomech. Abstr.* **1991**, *28*, 333–336. [[CrossRef](#)]
14. Belem, T.; Homand-Etienne, F.; Souley, M. Quantitative Parameters for Rock Joint Surface Roughness. *Rock Mech. Rock Eng.* **2000**, *33*, 217–242. [[CrossRef](#)]
15. Yuan, W.; Liu, S.F.; Tan, H.H.; Niu, J.D.; Jiang, Z.L.; Li, X.L.; Peng, S.; Xue, Y.Y.; Wang, W.; Sun, X.Y. A new approach for quantifying the two-dimensional joint roughness coefficient (JRC) of rock joints. *Environ. Earth Sci.* **2021**, *80*, 1–13. [[CrossRef](#)]
16. Bandis, S.C.; Lumsden, A.C.; Barton, N.R. Fundamentals of rock joint deformation. *Int. J. Rock Mech. Min. Sci. Geomech. Abstr.* **1983**, *20*, 249–268. [[CrossRef](#)]
17. Vallier, F.; Mitani, Y.; Boulon, M.; Esaki, T.; Pellet, F. A Shear Model Accounting Scale Effect in Rock Joints Behavior. *Rock Mech. Rock Eng.* **2010**, *43*, 581–595. [[CrossRef](#)]
18. Pikens, J.R.; Gurland, J. *Metallographic Characterization of Fracture Surface Profiles on Sectioning Planes*; Brown University: Providence, RI, USA, 1976.
19. Zhao, K. Study on Morphological Characteristics and Shear Mechanics Characteristics of Coal Structural Plane (Dissertation). *Gen. Res. Inst. Coal Sci.* **2021**, *12*, 89–95.

Disclaimer/Publisher’s Note: The statements, opinions and data contained in all publications are solely those of the individual author(s) and contributor(s) and not of MDPI and/or the editor(s). MDPI and/or the editor(s) disclaim responsibility for any injury to people or property resulting from any ideas, methods, instructions or products referred to in the content.